JOURNAL OF INFORMATION SCIENCE AND ENGINEERING 29, 835-849 (2013)

DOI:10.1688/JISE.2013.29.5.3

Specularity Removal using Dark Channel Prior*

BEIJI ZOU, XIAOYUN ZHANG, SHENGHUI LIAO AND LEI WANG
School of Information Science and Engineering
Central South University
Changsha, 410083 P.R. China

The reflectance of inhomogeneous objects can be described as a linear combination of diffuse and specular reflection components. Most computer vision algorithms assume that visually observable surfaces consist only of diffuse reflection. The existence of specular reflection can be misleading to these computer vision algorithms. A new algorithm – dark channel prior based specularity removal is proposed for separating specular and diffuse reflection components on colorful surfaces from a single input image. The dark channel prior is applied to detect the specular pixels in the image. The maximum diffuse chromaticity of the diffuse pixels is propagated to their neighboring specular pixels after specularity have been detected. Specularity removal can be achieved by using the specular-to-diffuse mechanism. The experimental results show that the proposed algorithm obtain comparable results as the state-of-the-art reflection components separation methods with the merit of being computationally more efficient.

Keywords: specularity removal, specularity detection, chromaticity, dark channel prior, specular-to-diffuse mechanism

1. INTRODUCTION

Highlight is a major problem for many computer vision applications. The reflectance of inhomogeneous materials (including wood, plastics and other opaque nonconductors with uniform pigmentation) can be described as a linear combination of specular and diffuse reflection components [1]. However, various vision algorithms (*e.g.*, image segmentation, object recognition and tracking) assume that visually observable surfaces consist only of diffuse reflection. The performance of these vision algorithms will inevitably suffer from the existence of specularity. Therefore, the separation of reflection components is highly desired in these computer vision applications.

The separation of reflection components (also known as specularity detection and removal) is a challenging problem. In the literature, a few approaches for reflection components separation have been proposed. A recent in-depth survey is given by Artusi *et al*. [2]. Reflection components separation approaches can be roughly categorized into polarization based methods, multiple images based methods and single image based methods. Polarization based methods [3, 4] remove specularity through images taken under different polarizing angles. Multiple images based methods [5, 6] obtain more constraints from images captured under changing lighting directions or viewpoints. These methods are effective in separating diffuse and specular reflection components, but the need for an additional polarization filter or multiple images significantly narrows their applicability.

Received December 9, 2011; revised March 12, 2012; accepted May 20, 2012.
Communicated by Yung-Yu Chuang.
* This work was supported by the National Natural Science Funds of China (No. 60970098 and No. 61173122), the Doctoral Program Foundation of Institutions of Higher Education of China (No.20090162110055, No. 200805331107), Hunan Provincial Natural Science Foundation of China (No. 09JJ6102).

In addition to polarization based and multiple images based methods mentioned above, there has been considerable interest in single image based methods. Klinker *et al*. [7] showed that a color histogram of a uniform colored surface forms a T-shaped distribution, with specular and diffuse pixels forming two linear clusters respectively. This method was extended to handle highlight on textured surfaces by introducing color segmentation. Unfortunately, current color segmentation algorithms are non-robust for complex textured images. To mitigate this problem, Tan *et al*. [8] presented the specular-to-diffuse mechanism and an iterative technique to remove highlights effectively without explicit color segmentation. Yang *et al*. [9] proposed a faster method based on the specular-to-diffuse mechanism. However, Yang's approach [9] estimated the maximum diffuse chromaticity by applying bilateral filter to each pixel's maximum chromaticity iteratively. There are cases that the specular reflection is lightly reduced but not removed.

Instead of processing the whole image iteratively, our approach focuses on processing the specular pixels which located by the dark channel prior [10, 11] and the automatic thresholding [12, 13]. This enables our approach to run faster than both of Tan's approach [8] and Yang's approach [9]. Like their approaches, the specular-to-diffuse mechanism is used to separate the two reflection components in our approach. Therefore, it can produce impressive results as the previous methods. The process of reflection components separation is simplified. The implementation of our approach is much easier than the previous methods.

The dark channel prior is first proposed for haze removal. It is a kind of statistics of colorful surfaces images. The key observation of the dark channel prior is diffuse colorful surfaces lacking color in any color channel will contribute to low values in the dark channel. On the contrary, specular pixels have higher intensity in all of the three color channels. Therefore, in the resulting dark channel image, the specular pixels can be differentiated from their surrounding diffuse pixels due to their higher intensity. So it can be applied to detect highlight on colorful surfaces. It enables easy and fast detection of specularity.

Most of the methods that use a single input image are basically based on color information, one commonly used assumptions is the surface color is chromatic ($R \neq G \neq B$). As most of the methods that have only a single input image, our method deal with specular highlight on colorful surfaces.

The rest of the paper is organized as follows: section 2 presents the basics of the reflection components separation. The details of specularity detection and removal is described in section 3. Experimental results on synthetic and real scene images is presented in section 4. Finally, our conclusions is offered in section 5.

2. REFLECTION MODEL

In computer vision and computer graphics, the model widely used to describe the formation of a specular image is the dichromatic reflection model introduced by Shafer [1], which states that the reflected lights of inhomogeneous objects captured by a RGB camera are a linear combination of diffuse and specular reflection components:

$$\mathbf{I}(\mathbf{x}) = \mathbf{I}^D(\mathbf{x}) + \mathbf{I}^S(\mathbf{x}) = \omega_d(\mathbf{x})\mathbf{B}(\mathbf{x}) + \omega_s(\mathbf{x})\mathbf{G}. \tag{1}$$

Where $\mathbf{I}$ is the observed image intensity, $\mathbf{x} = \{x, y\}$ is the image coordinates, $\mathbf{I}^D$ is the diffuse reflection component, $\mathbf{I}^S$ is the specular reflection component, $\mathbf{B}(\mathbf{x})$ is the diffuse color, $\mathbf{G}$ is the specular color, $\omega_d(\mathbf{x})$ and $\omega_s(\mathbf{x})$ represent coefficients that govern the magnitude of diffuse and specular reflection components respectively .

Let chromaticity be defined as:

$$\boldsymbol{\sigma}(\mathbf{x}) = \frac{\mathbf{I}(\mathbf{x})}{I_r(\mathbf{x}) + I_g(\mathbf{x}) + I_b(\mathbf{x})}. \tag{2}$$

Where $\boldsymbol{\sigma} = \{\sigma_r, \sigma_g, \sigma_b\}$. We define diffuse chromaticity $\boldsymbol{\Lambda}$ and illumination (specular) chromaticity $\boldsymbol{\Gamma}$ as follows:

$$\boldsymbol{\Lambda}(\mathbf{x}) = \frac{\mathbf{B}(\mathbf{x})}{B_r(\mathbf{x}) + B_g(\mathbf{x}) + B_b(\mathbf{x})}, \tag{3}$$

$$\boldsymbol{\Gamma} = \frac{\mathbf{G}}{G_r + G_g + G_b}. \tag{4}$$

With the definition in Eqs. (3) and (4), the dichromatic reflection model Eq. (1) can be written in terms of chromaticity:

$$\mathbf{I}(\mathbf{x}) = m_d(\mathbf{x})\boldsymbol{\Lambda}(\mathbf{x}) + m_s(\mathbf{x})\boldsymbol{\Gamma} \tag{5}$$

where

$$m_d(\mathbf{x}) = \omega_d(\mathbf{x})[B_r(\mathbf{x}) + B_g(\mathbf{x}) + B_b(\mathbf{x})], \tag{6}$$
$$m_s(\mathbf{x}) = \omega_s(\mathbf{x})[G_r + G_g + G_b]. \tag{7}$$

Assumed that the illumination chromaticity can be estimated by using a color constancy method [14]. Then the input image can be normalized such that $\Gamma_r = \Gamma_g = \Gamma_b = 1/3$. The diffuse component can be obtained by subtracting the specular component from the normalized input image.

$$\mathbf{I}^D(\mathbf{x}) = m_d(\mathbf{x})\boldsymbol{\Lambda}(\mathbf{x}) = \mathbf{I}(\mathbf{x}) - m_s(\mathbf{x})/3 \tag{8}$$

Following the definition of chromaticity and diffuse chromaticity above, we define maximum chromaticity and maximum diffuse chromaticity as follows:

$$\sigma_{\max} = \max(\sigma_r, \sigma_g, \sigma_b), \tag{9}$$
$$\Lambda_{\max} = \max(\Lambda_r, \Lambda_g, \Lambda_b). \tag{10}$$

3. DARK CHANNEL PRIOR BASED SPECULARITY REMOVAL

The flowchart in Fig. 1 illustrates the basic idea of our proposed method. We use the dark channel prior and the automatic thresholding to locate the specular pixels in the in-

put image. A binary mask with one denotes the specular pixels' location and zero denotes the diffuse pixels' location is generated by the end of specularity detection. By applying a propagation operation to the maximum chromaticity under the guidance of the mask image, we can estimate the maximum diffuse chromaticity. With the specular-to-diffuse mechanism, the estimated maximum diffuse chromaticity and the input image, specularity removal can be achieved.

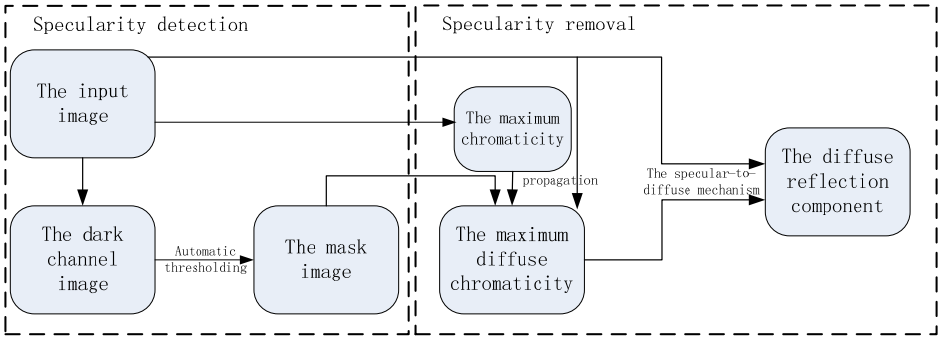

Fig. 1. Flowchart of the proposed method.

3.1 Specularity Detection

3.1.1 Dark channel image

To detect the specular pixels in the input image, we rely on the dark channel prior. The dark channel prior is first proposed by He *et al.* in [10, 11]. It is based on the observation that in most of the nonsky outdoor haze-free images patches, at least one color channel has very low intensity at some pixels. Formally, for an image **I**, a dark channel I^{dark} of **I** can be defined as follows:

$$I^{dark}(\mathbf{x}) = \min_{\mathbf{y}\in\Omega(\mathbf{x})}\left(\min_{c\in\{r,g,b\}}(I^{c}(\mathbf{y}))\right). \tag{11}$$

Where $\mathbf{\Omega}(\mathbf{x})$ is a local patch centered at $\mathbf{x}$, $\mathbf{x} = \{x, y\}$ is the image coordinates, I^c is a color channel of **I**.

With the concept of a dark channel in Fig. 2 (c), the dark channel prior states that if **I** is an outdoor haze-free image, for the nonsky region, the intensity of **I**'s dark channel is low and tends to be zero:

$$I^{dark} \to 0. \tag{12}$$

The low intensity in the dark channel is mainly due to three factors: shadows, colorful objects or surfaces and dark objects or surfaces.

To verify the fitness of the dark channel prior to the specularity removal problem, we collect 5,000 images from the Internet. Like most of the reflection components sepa-

ration method, our method only deals with highlight on the colorful surfaces. Therefore, all images in our image set are diffuse only colorful inhomogeneous material surfaces. The images are resized to make sure the maximum of width and height is 500 pixels and their dark channels are computed using a patch size of 3*3. Fig. 3 shows several colorful images and the corresponding dark channels.

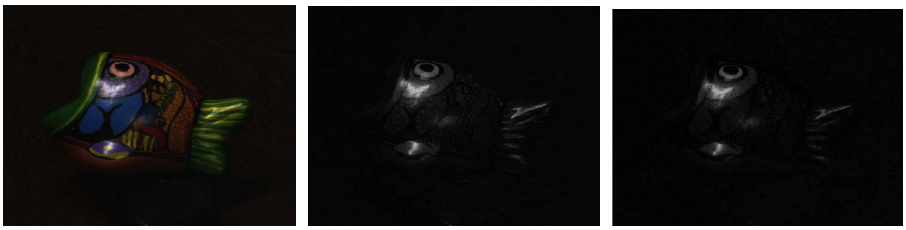

(a) (b) (c)

Fig. 2. Calculation of a dark channel; (a) An arbitray image I; (b) For each pixel, we take the minimum of its (r, g, b) value; (c) A minimum filter is performed on (b) to get the dark channel of I. The image size is 640*480, the patch size of Ω is 3*3.

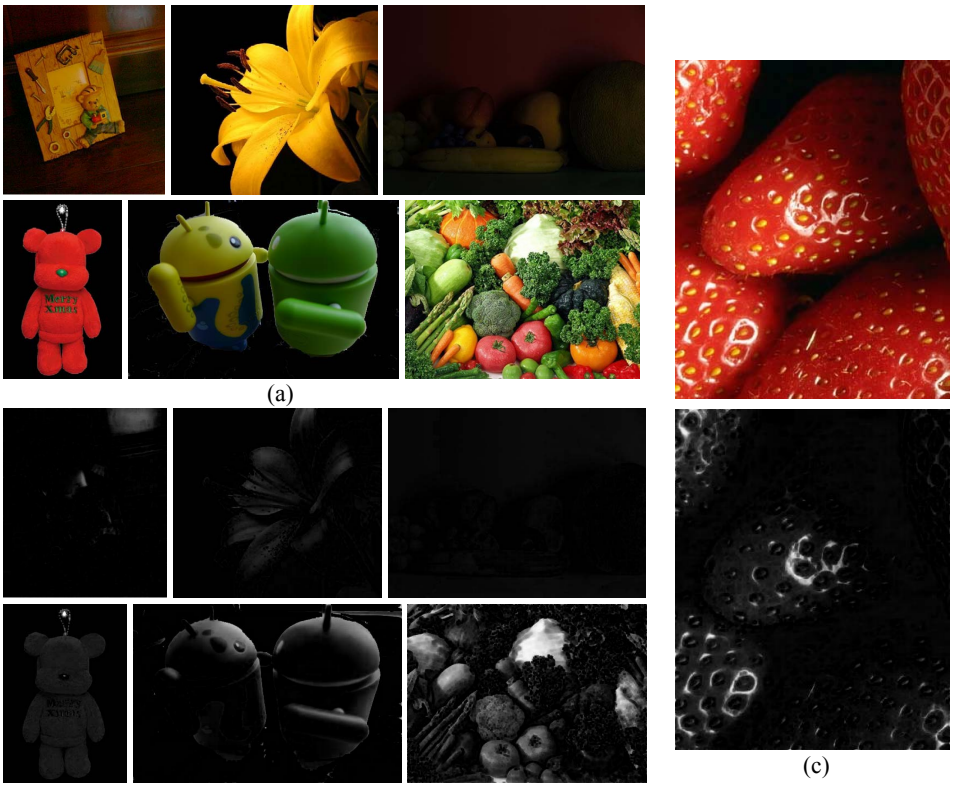

(a) (b) (c)

Fig. 3. (a) Example images in our specular-free colorful surface image database; (b) The corresponding dark channels; (c) A specular image and its dark channel.

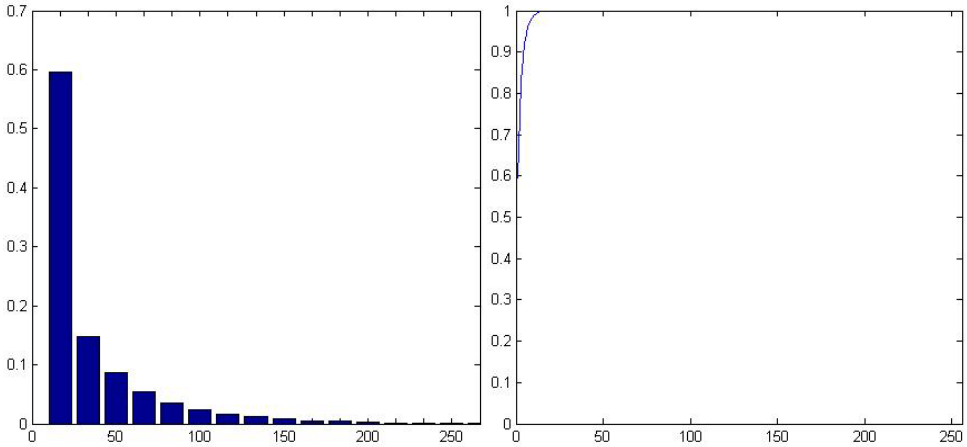

(a) (b)

Fig. 4. Statistics of the dark channels; (a) Histogram of the intensity of the pixels in all of the 5000 dark channels; (b) The cumulative distribution.

Fig. 4 (a) is the intensity histogram over all 5,000 dark channels, each bin stands for 16 intensity levels. Fig. 4 (b) is the corresponding cumulative distribution. We can see that the intensity of approximately 70 percent of pixels is below 20. This statistics gives strong support to the fitness of the dark channel prior to the specularity removal problem.

To this end, the diffuse colorful surfaces lacking color in any color channel will result in low values in the dark channel. Surface color discontinuities generally presents difficulties for specularity detection. Since it is colorful, it has low value in the dark channel. The specular pixels have higher intensity in three color channels, which will contribute to higher values in the dark channel. Therefore, the specular pixels are differentiated from the surrounding diffuse pixels due to their higher intensity in the dark channel image. The specular pixels can be located by thresholding the dark channel image. Fig. 2 (a) is an image with specularity and Fig. 2 (c) is the corresponding dark channel image (with patch size of 3*3). From Fig. 2 (c), we can see that the specularity becomes quite apparent in the dark channel image while the details of the textures and boundaries become less obvious.

Patch size in Eq. (11) is an important parameter for computing image dark channel. As authors of [10, 11] had pointed out a larger patch size was better for the dark channel prior. Because the probabilitity for a patch containing a dark pixel increased as the patch grows larger. However, in context of images with specularity on colorful surfaces, experiment results show that for such kind of images dark channel prior assumption is applicable with small patch size (Fig. 4). Furthermore, there exists small specular patches in specular images. These small patches would be missed if a larger patch size were used. Fig. 5 shows specularity detection results using different patch size. In Fig. 5 (b), the patch size is 3*3. Specular patches were detected accurately. While in Fig. 5 (c), the patch size is 15*15. Only large specular patches were marked out. In our implementation, we generally use a patch size of 3*3. Results show that our method works well when small patch size is used. When all specular patches are large and surfaces are light colored, we use a larger patch size.

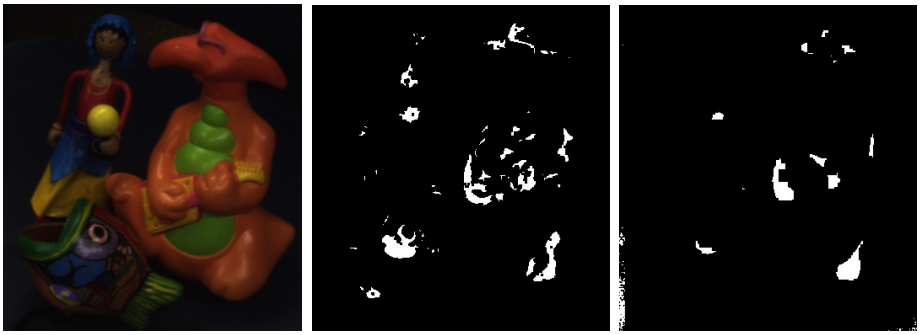

(a) (b) (c)

Fig. 5. (a) A 387*353 image with specularity and specularity masks detected using patch size of (b) 3*3 and (c) 15*15 respectively.

3.1.2 Automatic thresholding

Pixels in a specular image can be classified into specular pixels and diffuse pixels by using simple thresholding to the corresponding dark channel image. In our implementation, we apply the automatic thresholding [13] to a dark channel image to obtain a threshold value. A commonly used thresholding technique is the Otsu method [12] which selects threshold value that maximize the between-class variances of a histogram. It can provide satisfactory results for images with bimodal distribution histogram. However, the histogram of the dark channel image of a specular image is close to unimodal (Fig. 6 (a)) . The specular pixels generally consist of the minor portion of an image. They have higher intensity values in the dark channel image. The desired threshold value exists at the right bottom rim of the single peak of the dark channel image histogram. Therefore, the valley-emphasis method [13], a revised version of the Otsu's automatic thresholding method is used to select the threshold value (Fig. 6 (a)). The valley-emphasis method selects a threshold value that has a small probability of occurrence (valley in the histogram).

The formulation for the valley-emphasis method is:

$$t^* = ArgMax\{(1-p_t)(\omega_1(t)\mu_1^2(t)+\omega_2(t)\mu_2^2(t))\}. \tag{13}$$

Where t is a threshold value, p_t is the probability of occurrence at threshold value t. The smaller the p_t is, the larger the weight will be. Therefore, the weight ensures the resulting threshold value resides at the bottom rim of a unimodal histogram.

A mask image is generated by thresholding the dark channel image. We use one to represents specular pixels and zero to denote diffuse pixels in the mask image. The result of specularity detection of Fig. 2 (a) is shown in Fig. 6 (b).

$$mask(\mathbf{x}) = \begin{cases} 1 & \text{if I(x)} > t^* \\ 0 & \text{otherwise} \end{cases} \tag{14}$$

Where *mask* is the mask image, t^* is the threshold in Eq. (13).

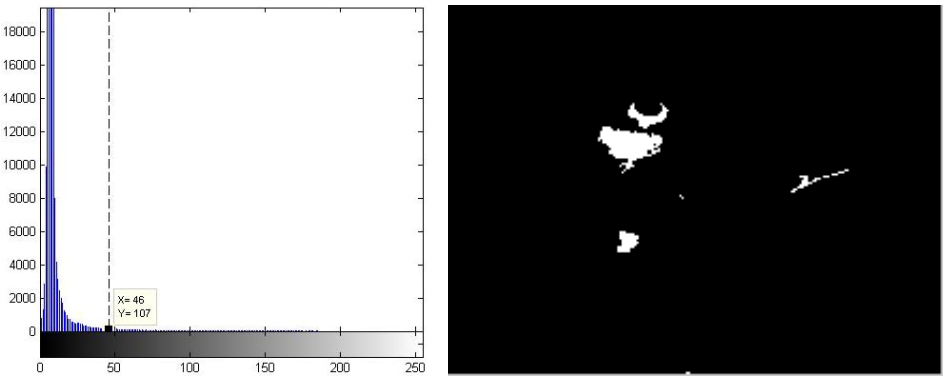

(a) (b)

Fig. 6. (a) The histogram of the dark channel image and the threshold; (b) The mask image.

3.2 Specularity Removal

The specular-to-diffuse mechanism is introduced by Tan *et al*. [8]. According to the specular-to-diffuse mechanism, a diffuse image $\mathbf{I}^D$ (image without specularity) can be derived as a non-linear function of the maximum diffuse chromaticity $\Lambda_{\max}$ (see Appendix A for complete derivation):

$$\mathbf{I}^D(\Lambda_{\max}) = \mathbf{I} - \frac{\max_{u\in(r,g,b)} I_u - \Lambda_{\max}\sum_{u\in(r,g,b)} I_u}{1-3\Lambda_{\max}}. \tag{15}$$

So the objective of removing specularity is reduced to estimate the maximum diffuse chromaticity of the input image.

The difference between the maximum chromaticity $\sigma_{\max}$ and the maximum diffuse chromaticity $\Lambda_{\max}$ is the specular pixels which featured by their lower the maximum chromaticity (the darker pixels in Fig. 7 (a) for instance). After specularity detection, the specular pixels have been marked out by the mask image. So we use the mask image to guide the estimating process of the maximum diffuse chromaticity. To estimate the maximum diffuse chromaticity, we propagate the maximum chromaticity of diffuse pixels to their nearby specular ones. Considering the specular patches may cover regions of different chromaticity (Fig. 7 (a)), we use a similar technique to [15] to detect boundaries.

$$(\Delta r > thR \text{ and } \Delta g > thG)\begin{cases} true: boundaries \\ false: otherwise \end{cases} \tag{16}$$

where $\Delta r(\mathbf{x}) = \sigma_r(\mathbf{x}) - \sigma_r(\mathbf{x}-\mathbf{1})$ and $\Delta g(\mathbf{x}) = \sigma_g(\mathbf{x}) - \sigma_g(\mathbf{x}-\mathbf{1})$ with $\sigma_r = I_r/(I_r + I_g + I_b)$, $\sigma_g = I_g/(I_r + I_g + I_b)$. thR and thG are scalars. Therefore the estimation of the maximum diffuse chromaticity can be defined as follows:

$$\tilde{\Lambda}(\mathbf{x}) = \begin{cases} \sigma_{\max}(\mathbf{x}) & \text{if } mask(\mathbf{x}) = 0 \text{ or boundaries} \\ \max(\sigma_{\max}(\mathbf{x}), \sigma_{\max}(\mathbf{x}-\mathbf{1})) & \text{otherwise} \end{cases}. \tag{17}$$

Where $\tilde{\Lambda}(\mathbf{x})$ is the estimated maximum diffuse chromaticity. To diffuse pixels and boundaries between different chromaticity regions, we set the estimated maximum diffuse chromaticity to the maximum chromaticity. For the rest of specular pixels, we compare the maximum chromaticity of a pixel (located in $\mathbf{x}$) with its neighbours (located in $\mathbf{x} - \mathbf{1}$) and choose the larger one to be the estimated maximum diffuse chromaticity of the pixel located in $\mathbf{x}$. The propagation process is summarized in Algorithm 1.

Algorithm 1: Estimating the maximum diffuse chromacity using a propagation process

```
1. Compute mask(section 3.1).
2. Compute σ_max using the input image I.
3. Let Λ̃ = σ_max.
4. for each pixel x
5.     if mask(x) == 1
6.             – compute Δr(x) and Δg(x)
7.             – if (Δr > thR and Δg > thG)
8.                 next x
9.             – else
10.                – Let Λ̃(x) = max(σ_max(x), σ_max(x – 1))
11.            – end
12.    end
13. end
14. apply Gaussian filter to Λ̃
15. return Λ̃.
```

In our experiments, we set thR and thG with the same number ranging from 0.003 to 0.05. The estimated maximum diffuse chromaticity may have some discontinuities on the boundaries of specular patches. We use a Gaussian filter to smooth it. The Gaussian filter parameters – scale and sigma are set to 3. Fig. 7 (b) presents the estimated maximum diffuse chromaticity $\tilde{\Lambda}$ of Fig. 2 (a). From it we can see that the propogation process works well when the specular patches cover different chromaticity. Substitute the estimated maximum diffuse chromaticity and the input image $\mathbf{I}$ into the Eq. (15), we can get the diffuse image in Fig. 7 (c). The specular component (Fig. 7 (d)) can be obtained by subtracting the diffuse component from the input image.

4. EXPERIMENTAL RESULTS

Our method is implemented and evaluated on a PC with 2.1GHz Intel Core 2 CPU processors and 2GB RAM.

Figs. 7-12 show some results of our method applied to synthetic and real scene images. As evaluated in [9], Yang's [9] method runs 200X faster than Tan's [8] method. Table 1 compares the runtime of Yang's [9] method and the proposed method using the images provided by authors of [8] and [9]. Our method is generally faster than Yang's [9] method while maintaining the visual effect.

From Fig. 7 (c) we can see that the specularity has been removed and the textures

are well preserved. Fig. 8 (a) is a synthetic image. Our result is close to Yang's [9] result and better than Tan's [8] result. In Figs. 9 and 10, the diffuse component in our result is comparable to Tan's [8] result and Yang's [9] result. Fig. 11 shows that our method successfully separated diffuse and specular components as Yang's [9] method did. From Fig. 12 we can see that Yang's [9] result and our result are better than Tan's [8] result. Our result has a little artifact at the bottom of the image. The reason is our method mistaken those white pixels for specularity. The intensity difference between those white pixels and their surrounding pixels are below the thR and thG we set. For the white pixels on the green apple, our result is the closest to the ground truth image. While in Fig. 12 (c), Yang's [9] result contains artifacts on the pear and the green apple. Our method recovered the diffuse component on that part appropriately.

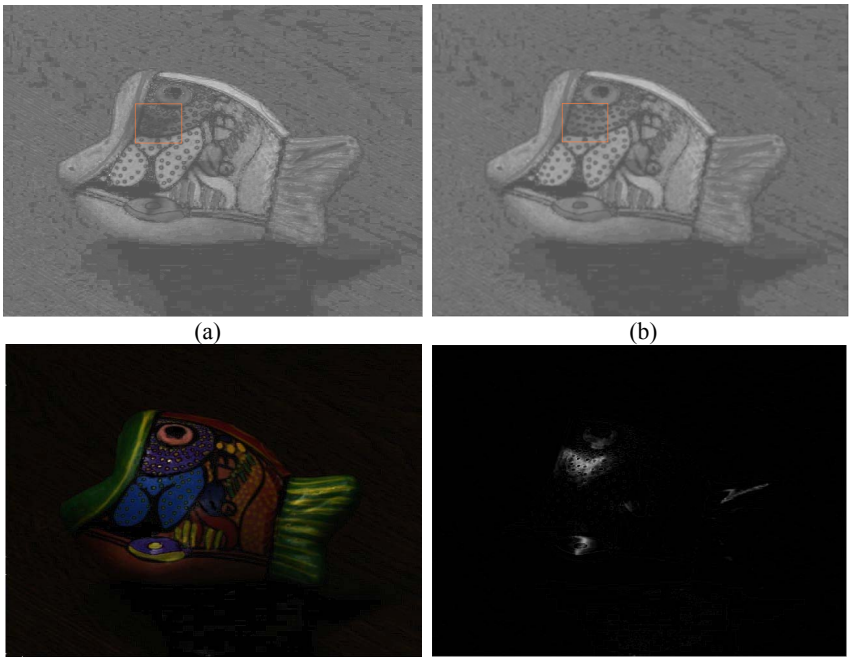

Fig. 7. (a) The maximum chromaticity of Fig. 2 (a); (b) The estimated maximum diffuse chromaticity of Fig. 2 (a); (c) The diffuse image of Fig. 2 (a); (d) The specular image of Fig. 2 (a).

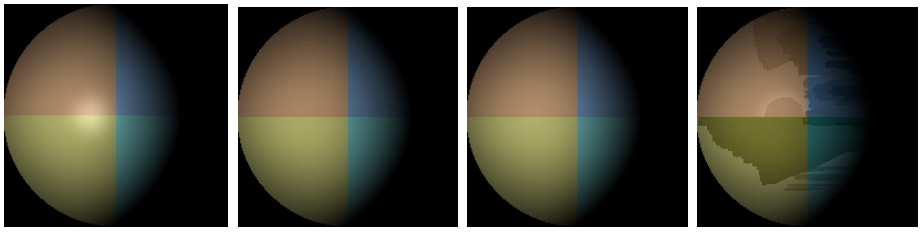

Fig. 8. (a) The input synth image; (b) The diffuse component (ours); (c) The diffuse component (Yang [9]); (d) The diffuse component (Tan [8]).

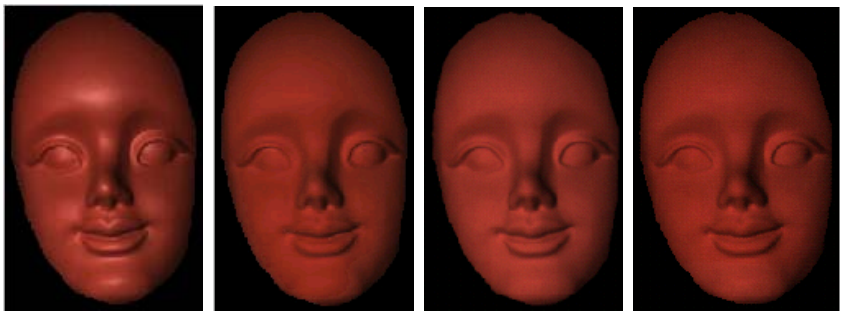

(a) (b) (c) (d)

Fig. 9. (a) The input head image; (b) The diffuse component (ours); (c) The diffuse component (Yang [9]); (d) The diffuse component (Tan [8]).

(a) (b) (c) (d)

Fig. 10. (a) The input toys image; (b) The diffuse component (ours); (c) The diffuse component (Yang [9]); (d) The diffuse component (Tan [8]).

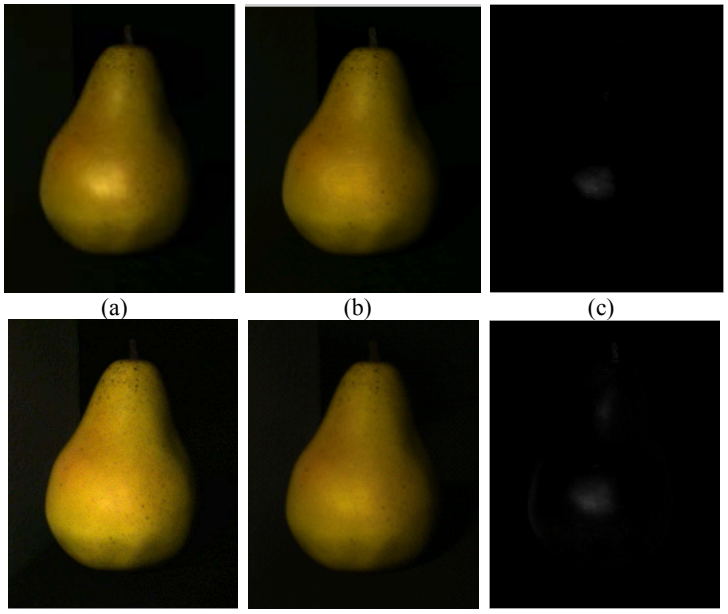

(a) (b) (c)

(d) (e) (f)

Fig. 11. (a) The input pear image; (b) The diffuse component (ours); (c) The specular component (ours); (d) The ground truth image; (e) The diffuse component (Yang [9]); (f) The specular component (Yang [9]).

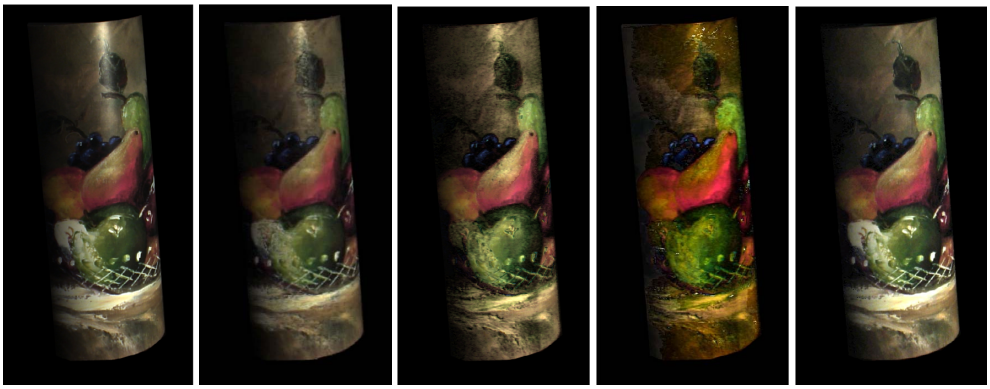

(a) (b) (c) (d) (e)

Fig. 12. (a) The input circle image; (b) The diffuse component (ours); (c) The diffuse component (Yang [9]); (d) The diffuse component (Tan [8]); (e) The ground truth.

Table 1. Speed comparison.

Image name (image size)	Our method	Yang's method
fish (640*480 pixels)	0.062s	0.110s
synth (200*200 pixels)	0.015s	0.015s
head (190*287 pixels)	0.016s	0.031s
pear (450*560 pixels)	0.047s	0.063s
toys (353*387 pixels)	0.032s	0.125s
circle (400*800 pixels)	0.094s	0.141s

5. CONCLUSION

In this paper, we have proposed a new specularity removal method using a single image. We use the dark channel prior and the automatic thresholding to detect the specular pixels. The maximum diffuse chromaticity of the detected specular pixels are estimated by propagating that of their nearby diffuse pixels. The specular-to-diffuse mechanism is applied to obtain the diffuse image from the input image. The proposed method offers some advantages. First, explicit color segmentation is avoided due to the use of the dark channel image. Surface color discontinuities which generally presents difficulties for specularity detection are become less apparent in the dark channel image. The specular pixels can be located by exploiting the fact that the specular pixels have higher intensity than their surrounding diffuse pixels. Therefore, the automatic thresholding can be used to detect specularity in the image. Second, the proposed method process only the specular pixels instead of the whole image and avoid iteration in estimating the maximum diffuse chromaticity, which enables our method to run faster. The experimental results demonstrate that the performance of our method is promising.

ACKNOWLEDGEMENTS

The authors thank the reviewers for providing insightful and valuable comments.

REFERENCES

1. S. Shafer, "Using color to separate reflection components," *Color Research and Applications*, Vol. 10, 1985, pp. 210-218.
2. A. Artusi, F. Banterle, and D. Chetverikov, "A survey of specularity removal methods," *Computer Graphics Forum*, Vol. 30, 2011, pp. 2208-2230.
3. L. B. Wolff, "Constraining object features using polarization reflectance model," *IEEE Transactions on Pattern Analysis and Machine Intelligence*, Vol. 13, 1991, pp. 635-657.
4. S. K. Nayar, X. S. Fang, and T. Boult, "Removal of specularities using color and polarization," in *Proceedings of IEEE Conference on Computer Vision and Pattern Recognition*, 1993, pp. 583-590.
5. S. W. Lee, "Detection of specularity using color and multiple view," *Image and Vision Computing*, Vol. 10, 1992, pp. 643-653.
6. S. Lin, Y. Li, B. S. Kang, and X. Tong, "Diffuse-specular separation and depth recovery from image sequences," in *Proceedings of Europe Conference of Computer Vision*, 2002, pp. 210-224.
7. G. J. Klinker, S. A. Shafer, and T. Kanade, "The measurement of highlights in color images," *International Journal of Computer Vision*, Vol. 2, 1990, pp. 7-32.
8. R. Tan and K. Ikeuchi, "Separating reflection components of textured surfaces using a single image," *IEEE Transactions on Pattern Analysis and Machine Intelligence*, Vol. 27, 2005, pp. 178-193.
9. Q. Yang, S. Wang, and N. Ahuja, "Real-time specular highlight removal using bilateral filtering," in *Proceedings of European Conference on Computer Vision*, 2010, pp. 87-100.
10. K. He, J. Sun, and X. Tang, "Single image haze removal using dark channel prior," in *Proceedings of IEEE Conference on Computer Vision and Pattern Recognition*, 2009, pp. 1956-1963.
11. K. He, J. Sun, and X. Tang, "Single image haze removal using dark channel prior," *IEEE Transactions Pattern Analysis and Machine Intelligence*, Vol. 33, 2011, pp. 2341-2353.
12. N. Ostu, "A threshold selection method from gray-level histograms," *IEEE Transactions on Systems*, *Man*, *Cybernet*, Vol. 9, 1979, pp. 62-66.
13. H. F. Ng, "Automatic thresholding for defect detection," *Pattern Recognition Letters*, Vol. 27, 2006, pp. 1644-1649.
14. R. Tan, K. Nishino, and K. Ikeuchi, "Illumination chromaticity estimation using inverse intensity chromaticity space," in *Proceedings of IEEE Conference on Computer Vision and Pattern Recognition*, 2003, pp. 673-680.
15. B. V. Funt, M. Drew, and M. Brockington, "Recovering shading from color images," in *Proceedings of European Conference on Computer Vision*, 1992, pp. 124-132.

APPENDIX A

According to the definition of the maximum chromaticity $\sigma_{\max}$ in Eq. (9) and the di-

chromatic reflection model which written in terms of the chromaticity in Eq. (5), we obtain

$$\sigma_{\max} = \frac{\max(I_r, I_g, I_b)}{I_r + I_g + I_b} = \frac{m_d(\mathbf{x})\mathbf{\Lambda}_{\max}(\mathbf{x}) + \frac{1}{3} m_s(\mathbf{x})}{m_d(\mathbf{x})[\mathbf{\Lambda}_r(\mathbf{x}) + \mathbf{\Lambda}_g(\mathbf{x}) + \mathbf{\Lambda}_b(\mathbf{x})] + m_s(\mathbf{x})} \tag{17}$$

since $\mathbf{\Lambda}_r(\mathbf{x}) + \mathbf{\Lambda}_g(\mathbf{x}) + \mathbf{\Lambda}_b(\mathbf{x}) = 1$, then we can get

$$m_s = m_d \frac{\Lambda_{\max} - \sigma_{\max}}{\sigma_{\max} - 1/3}. \tag{18}$$

Substitute m_s in the above equation into Eq. (5), we can obtain:

$$I_{\max}(\mathbf{x}) = m_d(\mathbf{x})(\mathbf{\Lambda}_{\max}(\mathbf{x}) - 1/3)(\frac{\sigma_{\max}(\mathbf{x})}{\sigma_{\max}(\mathbf{x}) - 1/3}), \tag{19}$$

then

$$m_d(\mathbf{x}) = \frac{I_{\max}(\mathbf{x})[3\sigma_{\max}(\mathbf{x}) - 1]}{\sigma_{\max}(\mathbf{x})[3\mathbf{\Lambda}_{\max}(\mathbf{x}) - 1]}. \tag{20}$$

Substitute the maximum chromaticity $\sigma_{\max}$ in Eq. (9) into the above equation,

$$m_d(\mathbf{x}) = \frac{3I_{\max}(\mathbf{x}) - \Sigma_{u\in(r,g,b)} I_u}{3\mathbf{\Lambda}_{\max}(\mathbf{x}) - 1}. \tag{21}$$

Since $m_s(\mathbf{x}) = \Sigma_{u\in(r,g,b)} I_u - m_d(\mathbf{x})$, combined with Eq. (21), the following equation can be obtained:

$$m_s(\mathbf{x}) = \frac{3(\Lambda_{\max}(\mathbf{x})\Sigma_{u\in(r,g,b)} I_u - \max_{u\in(r,g,b)} I_u)}{3\Lambda_{\max}(\mathbf{x}) - 1}. \tag{22}$$

According to Eq. (8) $\mathbf{I}^D(\mathbf{x}) = \mathbf{I}^D(\mathbf{x}) - m_s(\mathbf{x})/3$, combined with the above equation, we can get:

$$\mathbf{I}^D(\mathbf{x}) = \mathbf{I} - \frac{\max_{u\in(r,g,b)} I_u - \Lambda_{\max} \Sigma_{u\in(r,g,b)} I_u}{1 - 3\Lambda_{\max}}. \tag{23}$$

Beiji Zou (鄒北驥) received the B.S. degree in Computer Science from Zhejing University, China, in 1982, received the M.S. degree from Tsinghua University specializing CAD and computer graphics in 1984, and obtained the Ph.D. degree from Hunan University in the field of control theory and control engineering in 2001. He is now a Professor in School of Information Science and Engineering, Central South University, Changsha, China. He has published more than 100 papers in international conferences and journals. His research interests include computer graphics, computer vision and multimedia processing.

Xiaoyun Zhang (張瀟云) received the B.E. and M.E. in Computer Science from Central South University of Forestry and Technology in 2005 and 2008. She is pursuing the Ph.D. degree in School of Information Science and Engineering, Central South University, Changsha, China. Her current research interests include specularity removal , color constancy and computer vision.

Shenghui Liao (廖勝輝) received the BS degree in 2003 and Ph.D. degree in 2008 at Department of Computer Science and Engineering from Zhejiang University, China. From 2008, he continued his research as a Postdoctoral Researcher at Zhejiang University. He is now an Associate Professor in Central South University, China. His research interests include image analysis, computer-aided surgery, and machine learning.

Lei Wang (王磊) received the B.S. degree in Material Science and engineering from Hunan University, China, in 2000, obtained the Ph.D. degree from Hunan University in the field of control theory and control engineering in 2007. He is now a Lecturer in School of Information Science and Engineering, Central South University, Changsha, China. He has published dozens of papers in international conferences and journals. His research interest includes computer graphics, computer vision and multimedia processing.